***Journal of the Argentine Chemical Society***

# REVERSIBLE MULTI-ELECTRON REDUCTION OF 9,11,20,22-TETRAAZA-TETRAPYRIDOPENTACENE (tatpp) AS AXIAL LIGAND IN THE $[(bpy)_2Ru(tatpp)]Cl_2$ COMPLEX

**Lezna, R. O.[b]; de Tacconi, N. R.[a]; Janaratne, T.[a]; Muñoz Zúñiga, J.[b] and MacDonnell F. M.[a]**

[a]*Department of Chemistry and Biochemistry, The University of Texas at Arlington, Arlington, TX 76019-0065, USA.*

[b]*INIFTA-CONICET, C. C. 16, Suc. 4, La Plata (B1906ZAA), Argentina*

*Received June 6, 2009. In final form July 1, 2009.*

***Dedicated to Prof. Enrique J. Baran on the occasion of his retirement***

## Abstract

The ruthenium complex, $[(bpy)_2Ru(tatpp)]^{2+}$ ($\mathbf{1}^{2+}$; bpy is 2,2'-bipyridine where tatpp is 9,11,20,22-tetraaza tetrapyrido[3,2-a:2'3'-c:3'',2''-l:2''',3''']-pentacene) is a promising candidate for homogeneous solar photocatalysis, based on the coupling of light absorption by the $(bpy)_2Ru^{2+}$ chromophore moiety with the tatpp ability to receive and reversible store electrons in aqueous media. In the present communication, a combination of spectroelectrochemistry and voltammetry was applied to compare the electroreduction processes of tatpp in complex $\mathbf{1}^{2+}$ and as a Zn-tatpp adduct. For complex $\mathbf{1}^{2+}$, the radical $[(bpy)_2Ru(tatpp^{\bullet-})]^{+}$($\mathbf{1}^{\bullet+}$) is the first electroreduced species that then converts to doubly-reduced, single-protonated $[(bpy)_2Ru(Htatpp^{-})]^{+}$ ($H\mathbf{1}^{+}$) and doubly-protonated $[(bpy)_2Ru(H_2tatpp)]^{2+}$($H_2\mathbf{1}^{2+}$) by subsequent electron transfer (ET) and proton transfer (PT) reactions. Contrastingly, spectroelectrochemistry of the Zn-tatpp adduct showed negligible

amounts of intermediate tatpp$^{\bullet-}$ radical and dominance of double reduced Zn-(Htatpp$^{-}$) and Zn($H_2$tatpp) species. Upon further electroreduction, doubly-reduced species form quadruply reduced, protonated species, in both systems. The four electrons uptake in complex $\mathbf{1}^{2+}$ is followed by a rapid homogeneous comproportionation reaction with the initial $\mathbf{1}^{2+}$ reactant leading to the regeneration of intermediate double-reduced species, $H_2\mathbf{1}^{2+}$, while no comporportionation occurs for Zn-tatpp because the reduced species are film-confined, that is, restrained to move to the bulk solution for encounter with the initial reactant.

**Keywords**: photocatalisis, renewable energy, solar hydrogen, spectroelectrochemistry, mechanisms.

## Resumen:

El complejo de rutenio, $[(bpy)_2Ru(tatpp)]^{2+}$ ($\mathbf{1}^{2+}$; bpy es 2,2'-bipiridilo donde tatpp es 9,11,20,22-tetraaza tetrapirido[3,2-a:2'3'-c:3",2"-l:2"',3"']-pentaceno,) es un candidato promisorio para fotocatálisis solar homogénea, considerando su habilidad para acoplar la absorción de luz por medio del cromóforo $(bpy)_2Ru^{2+}$ con la propiedad del grupo tatpp para recibir y almacenar reversiblemente electrones en medio acuoso. En este trabajo se empleó una combinación de espectroelectroquímica y voltametría para comparar los procesos de electroreducción de tatpp en el complejo $\mathbf{1}^{2+}$y en el aducto Zn-tatpp. En el caso del complejo $\mathbf{1}^{2+}$, el radical $[(bpy)_2Ru(tatpp^{\bullet-})]^{+}$($\mathbf{1}^{\bullet+}$) es el primer producto electroreducido que luego da lugar a la especie doble reducida, monoprotonada $[(bpy)_2Ru(Htatpp^{-})]^{+}$ ($H\mathbf{1}^{+}$) y a la doble protonada $[(bpy)_2Ru(H_2tatpp)]^{2+}$($H_2\mathbf{1}^{2+}$) por reacciones de transferencia de electrones (ET) y de protones (PT). Por el contrario, la espectroelectroquímica del aducto Zn-tatpp mostró cantidades mínimas del intermediario radical tatpp$^{\bullet-}$ con predominancia de las especies Zn-(Htatpp$^{-}$) y Zn($H_2$tatpp). En una electroreducción adicional las especies doble reducidas forman, en ambos sistemas, especies protonadas cuadruple reducidas. El almacenamiento de cuatro electrones en el complejo $\mathbf{1}^{2+}$es seguido por una rápida comproporcionación homogénea con el reactivo inicial $\mathbf{1}^{2+}$conduciendo a la regeneración del intermediario doble reducido $H_2\mathbf{1}^{2+}$mientras que Zn-tatpp no muestra tal comproporcionación debido a que las especies reducidas se encuentran confinadas en una película adsorbida, impedidas de moverse hacia el seno de la solución para reaccionar con el reactivo inicial.

**Palabras clave**: fotocatálisis, energías renovables, hidrógeno solar, espectroelectroquímica, mecanismos.

## Introduction

Molecular photocatalysts aimed to use solar energy to generate $H_2$ and/or to convert $CO_2$ in useful fuels such as methanol and methane have shown considerably interest in the past few years.[1-6] While the development of efficient water-splitting photocatalysts still confronts important challenges, one central issue is matching the one-photon/one-electron nature of most molecular photoexcitations with the multi-electron and multi-proton requirements of important fuel making reactions, such as hydrogen and oxygen evolution reactions. To date, only a few artificial photocatalysts have shown the ability to store multiple reducing or oxidizing equivalents via a photochemical process [7-15] even though such functionality is integral to photosystems in nature. Proton-transfer is also an essential feature of photoinduced electron-transfer processes in most natural light-activated energy storing processes [16,17]. Similarly, proton-transfer will play a central role in artificial photocatalysis. Therefore, it has become evident that a better understanding of the mechanisms of multi-electron and protonation processes is needed. [18,19]

We have previously shown that the dinuclear ruthenium(II) complexes, $[(phen)_2Ru(tatpp)Ru(phen)_2]^{4+}$ ($\mathbf{2}^{4+}$) and $[(bpy)_2Ru(tatpp)Ru(bpy)_2]^{4+}$ ($\mathbf{3}^{4+}$), are photochemically

active and both undergo two tatpp ligand-based reductions upon visible light irradiation in the presence of sacrificial donors. [7,20,21] The phenanthroline complex has also shown intriguing biological activity in that its doubly-reduced form cleaves DNA by a mechanism that appears to involve a carbon-centered radical intermediate. [22] We have also shown that the related mononuclear complexes, $[(bpy)_2Ru(tatpp)]^{2+}$ ($\mathbf{1}^{2+}$) and $[(phen)_2Ru(tatpp)]^{2+}$ show similar redox processes in MeCN, however, this redox chemistry is complicated by the spontaneous formation of π-stacked assemblies (instigated by easy overlap of flat tatpp ligands) in MeCN as well as the formation of σ bonded dimers between radical species.[23]

Aggregation and radical dimerization are not the dominant processes for $\mathbf{1}^{2+}$ during the electroreduction in aqueous solution unlike the situation in MeCN, instead the complex remains largely unaggregated in this media and the mechanistic details of the tatpp-based electroreduction and protonation are more easily examined. [24]

In this work, multi-electron reduction process of complex $\mathbf{1}^{2+}$ and a Zn-tatpp adduct are compared. The free tatpp ligand is insoluble in all common solvents and coordination to $Zn^{2+}$ is necessary for solubilization. Under these conditions of excess $Zn^{2+}$, it is likely that both ends are coordinated to $Zn^{2+}$ ions, however, for simplicity, we refer to the adduct as Zn-tatpp.

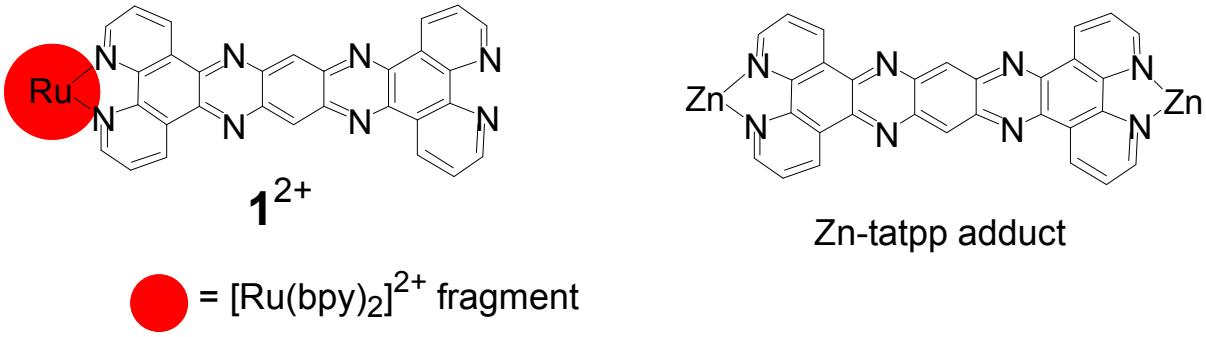


Coordination to $Zn^{2+}$ is not expected to significantly change the optical properties of the tatpp molecule but is likeky to perturb the redox potentials of the tatpp ligand, predominantly via electrostatic interactions. In contrast, $Ru^{2+}$ coordination to tatpp is a significantly more covalent interaction, leading to both electrostatic and orbital overlap perturbations to the redox processes of the tatpp ligand. Spectroelectrochemistry was used to determine the species formed during reversible multi-electron uptake in both systems. For the speciation of $\mathbf{1}^{2+}$ during electroreduction, basic aqueous solution were chosen to avoid radical dimerization, while for the Zn-tatpp adduct, an acetonitrile:water mixture with 10-fold molar excess of $Zn^{2+}$ to tatpp was used for solubility. In both scenarios, reversible uptake of four electrons is demonstrated although under different mechanisms that are clearly discerned with the assistance of spectroelectrochemical measurements.

## Experimental

Ruthenium complex $\mathbf{1}[PF_6]_2$ and the related water soluble $\mathbf{1}[Cl]_2$ were prepared by modifying a reported procedure [25] for the $[(phen)_2Ru(tatpp)]^{2+}$ complex using $[(bpy)_2Ru(1,10\text{-phenanthroline-5,6-dione})][PF_6]_2$ [26] in place of $[(phen)_2Ru(1,10\text{-phenanthroline-5,6-dione}][PF_6]_2$. Tatpp was prepared by a reported procedure.[27] Solubilization in acetonitrile was achieved with an excess of $Zn(BF_4)_2$ and ~10% water.

Electrochemical data were obtained on a CHI620C electrochemical analyzer (CH Instruments, Austin, TX, USA). A glassy carbon (1.5 mm diameter disk) working electrode from Cypress Systems was used. Immediately before use, the electrode was polished to a mirror finish

with wet alumina (Buehler, 0.05 μm), followed by rinsing with Millipore Milli-Q water and sonication. A Pt wire and a Ag/AgCl reference electrode (Cypress, model EE009) were used as counter and reference electrodes, respectively. For complex $\mathbf{1}^{2+}$, the electrolyte solutions were prepared from $NaH_2PO_4$/ $K_2HPO_4$ buffer, the pH was adjusted with 0.5 M NaOH; while for the tatpp molecule, 0.1 M tetrabutylammonium hexafluorophosphate ($TBAPF_6$) as supporting electrolyte in acetonitrile: $H_2O$ 90:10 was used. Prior to each measurement, solutions were deoxygenated by bubbling argon. This atmosphere was maintained over the electrochemical solution throughout the course of the experiment. All experiments pertain to the laboratory ambient temperature (20 ± 2 °C).

Cobaltocene ($Co(Cp)_2$) and trifluoroacetic acid (TFA), both from Alfa Aesar®, were used as received. All redox and protonation titrations were carried out in a nitrogen atmosphere glovebox using stock solutions of $\mathbf{1}[PF_6]_2$ ($10^{-4}$ M), $Co(Cp)_2$ (0.01 M), and TFA (0.01 M). Compounds $\mathbf{1}^{\bullet+}$ and $\mathbf{1}^0$ were generated by adding 1 and 2 equivalents of $Co(Cp)_2$, respectively. The protonated species were generated by stoichiometric addition of TFA to solutions of $\mathbf{1}^{\bullet+}$ and $\mathbf{1}^0$.

Two UV-visible spectroelectrochemical configurations were used: (a) Transmittance spectroelectrochemical measurements were performed under constant potential in a 4 mm-cuvette with a transparent indium tin oxide (ITO) film on a glass substrate as working electrode and presented as difference absorption spectra, ΔA, to boost the spectral changes occurring at the electrode/electrolyte interface. Spectroelectrochemical data was recorded as a function of time by using a diode array spectrometer (Hewlett-Packard model 8453). The counter electrode (platinum wire) and the Ag/AgCl reference microelectrode (Cypress model EE009) were laterally placed in the quartz cuvette next. (b) Reflectance measurements, using a mirror-polished gold electrode, were collected with an EG&G/PAR Optical Multichannel Analyzer, OMA, during a slow potential scan (5 mV/s), the data being presented as $\Delta R/R$ vs. potential at selected wavelengths. The reflectance changes, $\Delta R = R\text{-}R_0$, were measured with respect to the system reflectance at the initial potential ($R_0$) where no reactions are taking place.

## Results

Representative cyclic voltammograms for the electroreduction of complex $\mathbf{1}^{2+}$ and Zn-tatpp adduct are shown in Figure 1. For complex $\mathbf{1}^{2+}$, Figure 1a compares the effect of solvent, acetonitrile vs. water at pH 10.5, on the voltammetric profiles obtained with a glassy carbon electrode. Two main redox processes, $C_1/A_1$ and $C_2/A_2$ are at ca. the same potentials in both solvents, at -0.41 and -0.81 V respectively; however, the peak $C_1/A_1$ is better defined in aqueous media whereas in acetonitrile two overlapped monomer-dimer contributions are detected.[23] At potentials negative of -1.2 V the reversible redox processes related to the bipyridine ligands are observed; these peaks are not accessible in aqueous media due to the interference of the hydrogen evolution reaction. For the Zn-tatpp adduct, two redox processes are also observed at 0.02 V and -0.30 V respectively (Fig. 1b), significantly more positively located than in complex $\mathbf{1}^{2+}$. An additional redox couple (C'/A') is observed at more negative potentials and related to zinc reduction/stripping ($Zn^{2+}/Zn^0$) as $Zn(BF_4)_2$ is in excess concentration. Considering that the first two redox processes in complex $\mathbf{1}^{2+}$ (Figure 1a) and the Zn-tatpp adduct (Figure 1b) are associated to the electroreduction of the tatpp ligand, the more positive potentials in the Zn-tatpp adduct reveal less electron delocalization on the tatpp ligand by $Zn^{2+}$ relative to $Ru^{2+}$ which is consistent with strong π-backbonding in the Ru complex. Interestingly, upon repeated potential cycling the Zn-adduct forms an insoluble film on the electrode surface as seen in Figure 2. On the first 15 potential cycles (only the 1st, 7th and 15th cycles are shown for the sake of clarity), there is a progressively current increase of the two redox processes, after ca. 20 cycles the growth process slows down and the electrode surface is visible covered by a blue film. The gradual negative shift in the cathodic reduction potential suggests that some $Zn^{2+}$ demetallates in the process, as removal of $Zn^{2+}$ would

modify the potential negatively. The effectiveness of film growth, as measured by the increase of peak current, was found to depend on both the excess of $Zn^{2+}$ and the $TBAPF_6$ supporting electrolyte concentration. Decreasing the $TBAPF_6$ concentration from 0.1 to 0.03 M significantly decreases the film growth and finally films are not formed when the $TBAPF_6$ concentration is lower than ~0.03 M. This concentration dependence seems rooted in the necessity of charge compensation during the potentiodynamic film growth. In fact, the film requires the uptake of cations (most likely protons) during the electroreduction process and their release upon oxidation in order to compensate the charge generated by surface-confined electrochemical reactions. This electrochemical behavior is reminiscent of the potentiodynamic film growth of Prussian blue analogues [28-30] as well as that of conducting polymers, e.g. polyaniline and polypyrrole. [31-33]

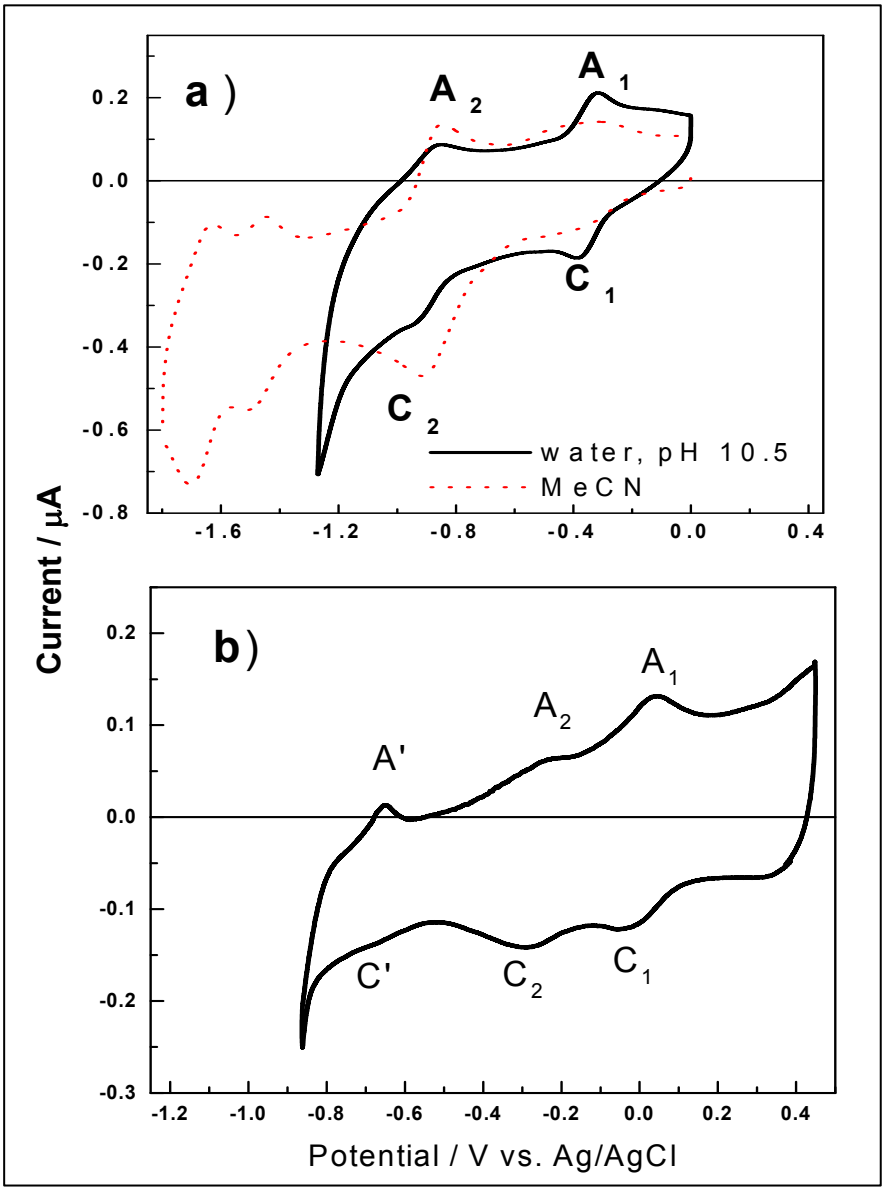


**Figure 1.** (a) Cyclic voltammograms at 20 $mV.s^{-1}$ for the electroreduction/electroxidation of complex $\mathbf{1}^{2+}$ (20 µM) on a glassy carbon electrode (1.5 mm dia.) in buffered pH 10.5 aqueous media (solid line, switching negative potential of -1.3 V) and in acetonitrile (dash line, switching negative potential of -1.8 V) respectively.
(b) Cyclic voltammogram at 40 $mV.s^{-1}$ for the electroreduction/electroxidation of Zn-tatpp (25 µM).

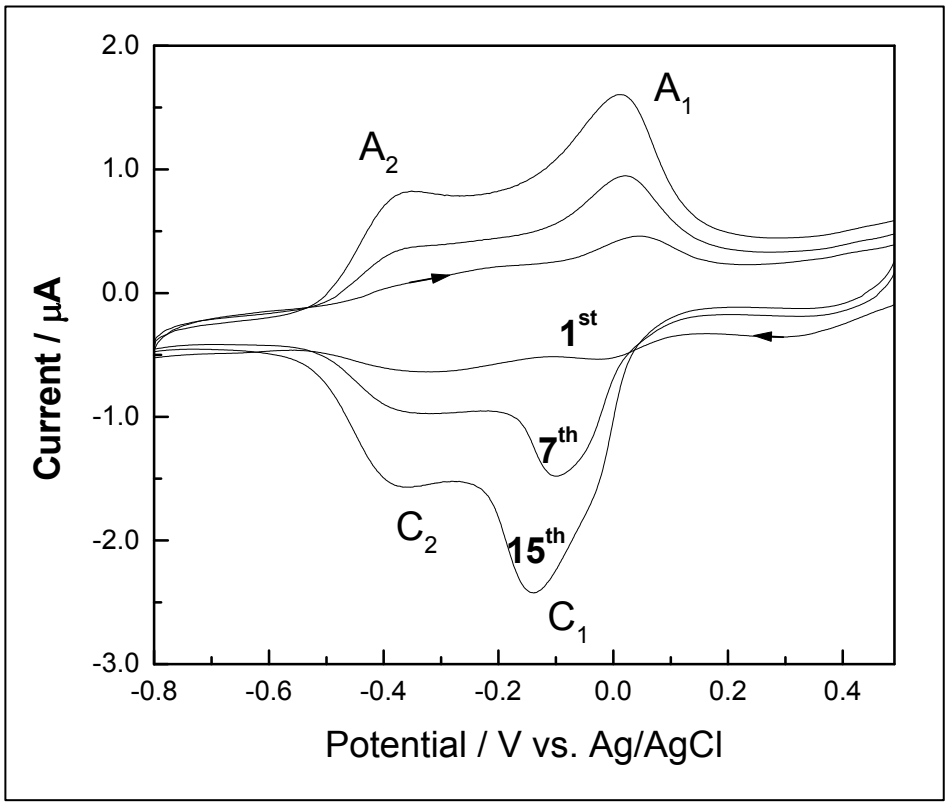


**Figure 2.** Selected cyclic voltammograms ($1^{st}$, $7^{th}$ and $15^{th}$) recorded during repetitive cycling at 100 $mV.s^{-1}$ of Zn-tatpp (100 μM) in 0.15 M $TBAPF_6$ using MeCN:$H_2O$ 90:10 and an ITO working electrode.

To identify the electrochemically formed species in $\mathbf{1}^{2+}$, we first performed in situ stoichiometric chemical reduction and protonation to generate a number of species singled out as likely products. These reactions were performed in dry MeCN to obtain the non-protonated reduced species, and then TFA was used for stoichiometric protonation. Figure 3 shows the absorption spectra of the non-protonated $\mathbf{1}^{2+}$, $[(bpy)_2Ru(tatpp^{\bullet-})]^{+}$($\mathbf{1}^{\bullet+}$), $[(bpy)_2Ru(tatpp^{2-})]$($\mathbf{1}^{0}$) and the related protonated species $[(bpy)_2Ru(Htatpp^{-})]^{+}$ ($H\mathbf{1}^{+}$), and $[(bpy)_2Ru(H_2tatpp)]^{2+}$($H_2\mathbf{1}^{2+}$) as obtained from titration with $Co(Cp)_2$ and TFA respectively. $Co(Cp)_2$ is a strong one-electron reducing agent ($E_0$ = -1.0 V vs. Ag/AgCl in acetonitrile)[34] and therefore thermodynamically capable of generating both $\mathbf{1}^{\bullet+}$ and $\mathbf{1}^{0}$ species.[23] The resulting cobaltocenium ion generated in the redox reaction features no appreciable absorption in the visible and near-IR portion (350-1100 nm) of the absorption spectra [35] and thus does not affect our spectra obtained in this region.

Spectrum of complex $\mathbf{1}^{2+}$ (Figure 3, solid line) contains the contribution of the tatpp ligand at 330 and 445 nm [21], overlapped with that of the $[Ru(bpy)_2]^{2+}$ chromophore moiety absorbing also at 445 nm. The radical $\mathbf{1}^{\bullet+}$, formed upon addition of one equivalent of $Co(Cp)_2$, shows two new absorptions in the near-IR at 855 nm (weak) and 960 nm (strong) plus a discernible band at 400 nm, as well as a partial disappearance of the absorption at 330 nm. The doubly reduced $\mathbf{1}^{0}$, obtained after addition of a second $Co(Cp)_2$ equivalent, shows a strong band at 692 nm with a shoulder at 642 nm (see Figure 3) and a partial bleaching of the 400 nm absorption. The doubly-reduced, single-protonated $H\mathbf{1}^{+}$, formed with TFA, is characterized by waves at 640 and 708 nm plus a faintly but discernible shoulder at ca. 605 nm, while the doubly-reduced, doubly-protonated $H_2\mathbf{1}^{2+}$ shows a broad absorption peaking at 565 nm (Figure 3).

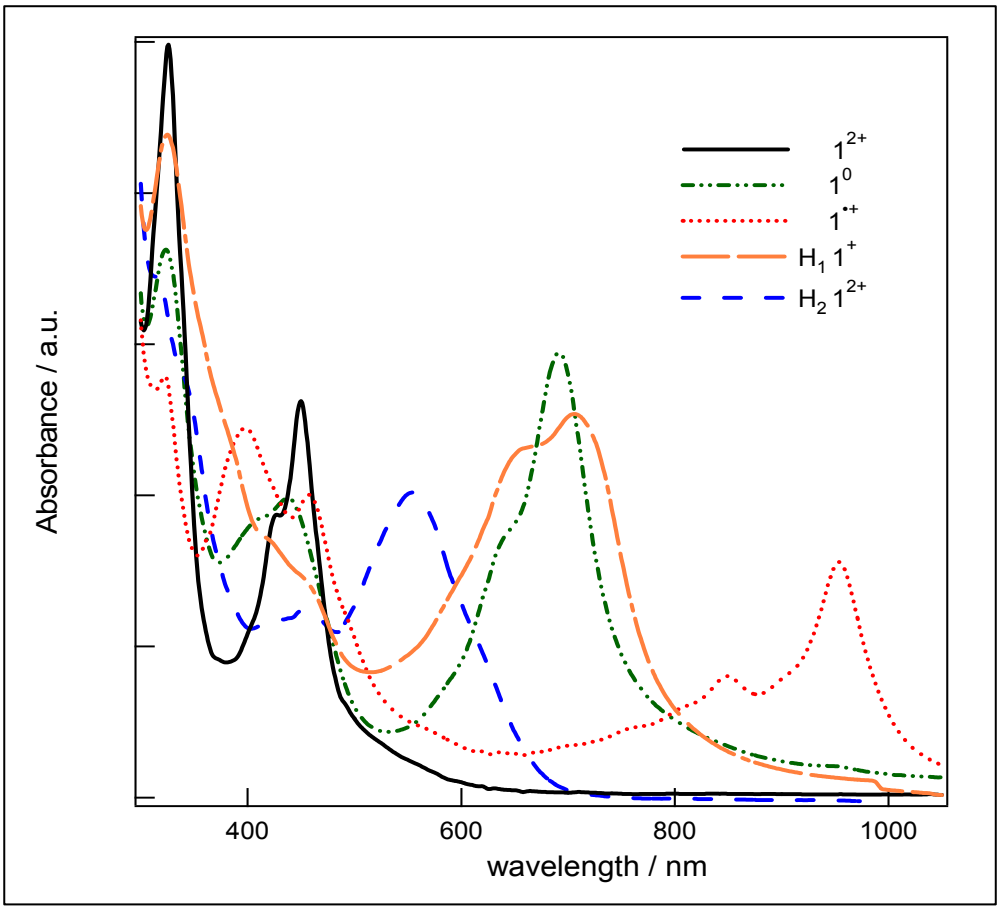


**Figure 3.** Electronic spectrum (MeCN) of $\mathbf{1}^{2+}$ (black line) and the resulting spectra after the addition of 1 and 2 equiv. of $Co(Cp)_2$, leading to the formation of species $\mathbf{1}^{\bullet+}$ (red dotted line) and $\mathbf{1}^{0}$ (green dash-dotted line) respectively. Spectra of $\mathbf{1}^{2+}$after the addition of 2 equiv of $Co(Cp)_2$ and 1 equiv of TFA ($H\mathbf{1}^{+}$ species, orange dash line) and 2 equiv of $Co(Cp)_2$ and 2 equiv of TFA ($H_2\mathbf{1}^{2+}$ species, blue dash line) respectively.

Spectroelectrochemical data of $\mathbf{1}^{2+}$ and Zn-tatpp are shown in Figures 4 and 5 respectively. Figure 4 shows the spectral evolution under a double potential step from 0.0 to -1.2 V and back to 0.0 V as difference absorption spectra, ΔA, using the absorbance at the initial potential as reference. A sketch of the potential waveform is included as inset in Figure 4a. The resulting spectra contain bands pointing up, for the appearance of new species in solution, whereas the opposite holds for bands pointing down. The top frame (Figure 4a) corresponds to the negative potential pulse (reduction), and the frame at the bottom (Figure 4b) was obtained during the subsequent, positive pulse (oxidation), with arrows in each frame indicating the time evolution of the corresponding spectral peaks. The similarity of the spectra profiles in Figures 4a (reduction) and 4b (oxidation) is clear evidence of the high electrochemical reversibility of complex $\mathbf{1}^{2+}$.

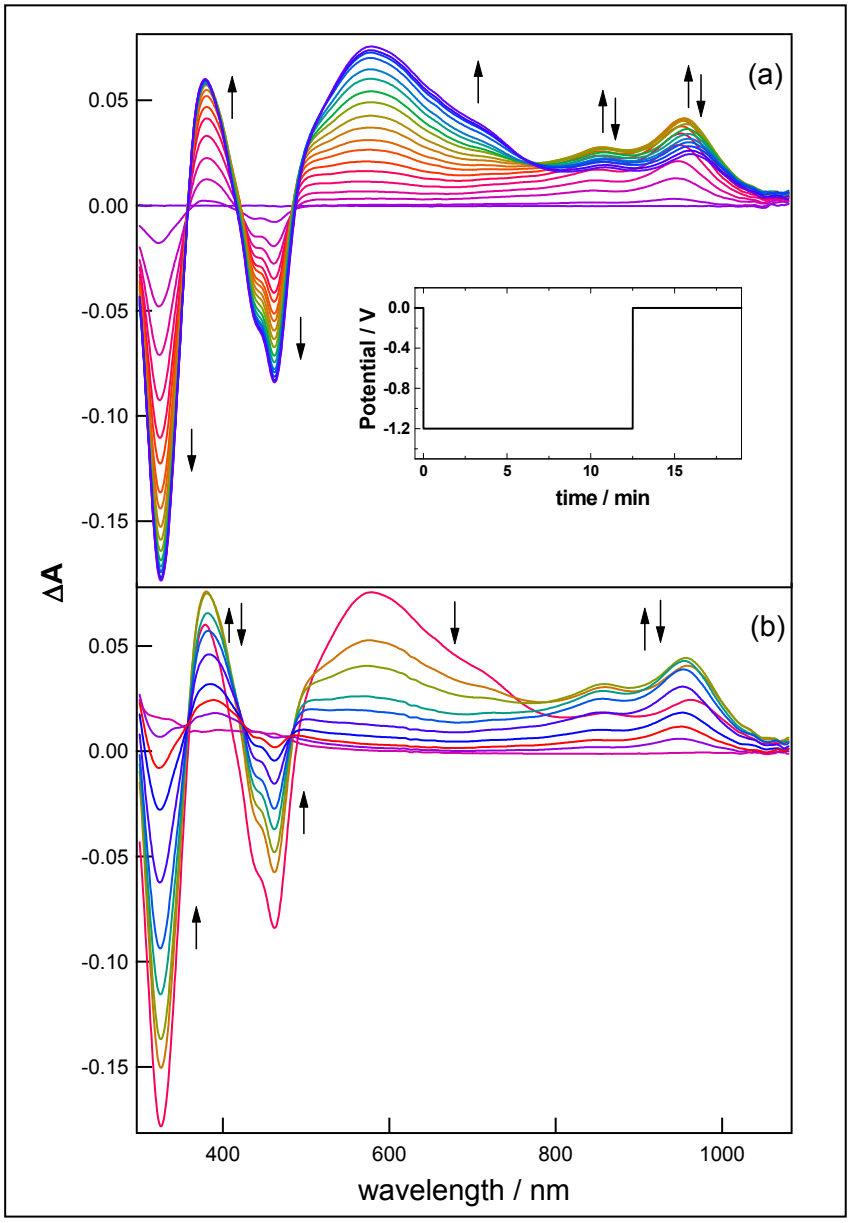


**Figure 4.** Difference absorbance spectra, **ΔA,** during the electroreduction and subsequent electrooxidation of $\mathbf{1}^{2+}$ (50 μM) in a 10.5 pH buffered aqueous solution subjected to a double potential step from 0.0 V to -1.2 V (a) and back to 0.0 V (b). The working electrode was a transparent ITO film on a glass substrate. The double-step potential waveform is shown in the inset in Figure 4a.

As seen in Figure 4a, during the electroreduction process the sharp absorptions at 330 and 455 nm are disappearing (bands pointing downwards) while two new spectral waves (pointing upwards) at 855 and 960 nm start growing. These two absorptions then transform into a broad absorption band at 565 nm with a shoulder at 712 nm. The spectroelectrochemical response at 855 and 960 nm is consistent with that obtained by $Co(Cp)_2$ reduction of $\mathbf{1}^{2+}$ to $\mathbf{1}^{\bullet+}$ (see Figure 3) and confirms that the two processes (electrochemical and chemical reduction) yield the same initial product. Likewise, the subsequent electrochemical formation of species peaking at 565 and 712 nm

(Figure 4a) is consisting with the spectra obtained by $Co(Cp)_2$ reduction/TFA protonation (Figure 3) revealing that doubly-reduced species are being electrochemically formed in two different protonation states, $H\mathbf{1}^{+}$ and $H_2\mathbf{1}^{2+}$. During the potential pulse from -1.2 V to 0.0 V, the $H\mathbf{1}^{+}$ and $H_2\mathbf{1}^{2+}$ (712 and 565 nm respectively) are seen to change into the formation of $\mathbf{1}^{\bullet+}$ (with absorptions at 855 and 960 nm), which, in turn, also disappears leading to $\Delta A \rightarrow 0$ in the whole spectral range. That is, the system is brought back to the initial $\mathbf{1}^{2+}$ species, whose spectrum was taken as reference (Figure 4b).

The absorbance (concentration) profiles for species $\mathbf{1}^{\bullet+}$ (855 nm) , $H\mathbf{1}^{+}$(712 nm) and $H_2\mathbf{1}^{2+}$ (565 nm) obtained from data in Figure 4 at selected wavelengths as a function of time at -1.2 V and at 0.0 V are shown in Figure 6. The amount of $\mathbf{1}^{\bullet+}$ species is firstly seen to grow with time at -1.2 V, goes over a maximum and decays through its transformation into $H\mathbf{1}^{+}$ and $H_2\mathbf{1}^{2+}$. In fact, the decrease in $\mathbf{1}^{\bullet+}$ concentration is clearly accompanied by the steady increase in both $H\mathbf{1}^{+}$ and $H_2\mathbf{1}^{2+}$ until the reversed potential (0.0V) leads to the regeneration of $\mathbf{1}^{\bullet+}$ at the expense of $H\mathbf{1}^{+}$ and $H_2\mathbf{1}^{2+}$ concentrations. Finally, radical $\mathbf{1}^{\bullet+}$ oxidizes to the initial $\mathbf{1}^{2+}$ in a relatively short time (~ 6 min). Although the kinetics to reach the steady-state condition is different for the two potentials, the related redox intermediates reappear (disappear) in order until $\mathbf{1}^{2+}$ is completely regenerated, that is the difference $A_{-1.2\ V} - A_{0.0\ V}$ returns to practically zero.

For the Zn-tatpp adduct, Figure 5 shows the difference absorption spectra, ΔA, recorded under two subsequent negative potentials steps encompassing the first ($C_1$) and second ($C_2$) electroreduction processes (see Figure 1b). The potential was stepped from the value at open circuit to –0.15 V (Figure 5a) and then to -0.8 V (Figure 5b). A sketch of the potential waveform is included as inset in Figure 5a. In the potential step to -0.15 V (Figure 5a), the first species formed is absorbing at 855 and 960 nm and corresponds to the formation of the Zn-tatpp$^{\bullet-}$ radical, however, this species is only detected in minor amounts (significantly lower than the related $\mathbf{1}^{\bullet+}$, see Figure 4a). The dominant species absorbs at 570, 638 and 692 nm and appears to be a mixture of the doubly-reduced Zn-(tatpp$^{2-}$) adduct in its singly Zn-(Htatpp$^{-}$) and doubly protonated Zn-($H_2$tatpp) forms. The appearance of well-resolved vibrational fine structure suggests Zn-(Htatpp$^{-}$) is the dominant species present as this fine structure is typically seen in the doubly-reduced, monoprotonated tatpp ligand in $\mathbf{1}^{2+}$ and $\mathbf{2}^{4+}$.[21, 23-24] These bands are significantly much thinner that those obtained in the related spectra for the electroreduction of complex $\mathbf{1}^{2+}$ (Figure 4a) a result that we attribute to solvent effects (tatpp cannot be solubilized in water in order to compare this behavior in the same media as for $\mathbf{1}^{2+}$). When the potential is changed to -0.8 V, i.e. passing the $C_2$ process, the absorptions at 570, 638 and 692 nm are seen to decrease during this second electroreduction process (Figure 5b). This behavior contrasts with the observation of a continuous build-up of doubly-reduced species during the electroreduction of complex $\mathbf{1}^{2+}$ at potentials passing the process $C_2$ (Figure 4a).

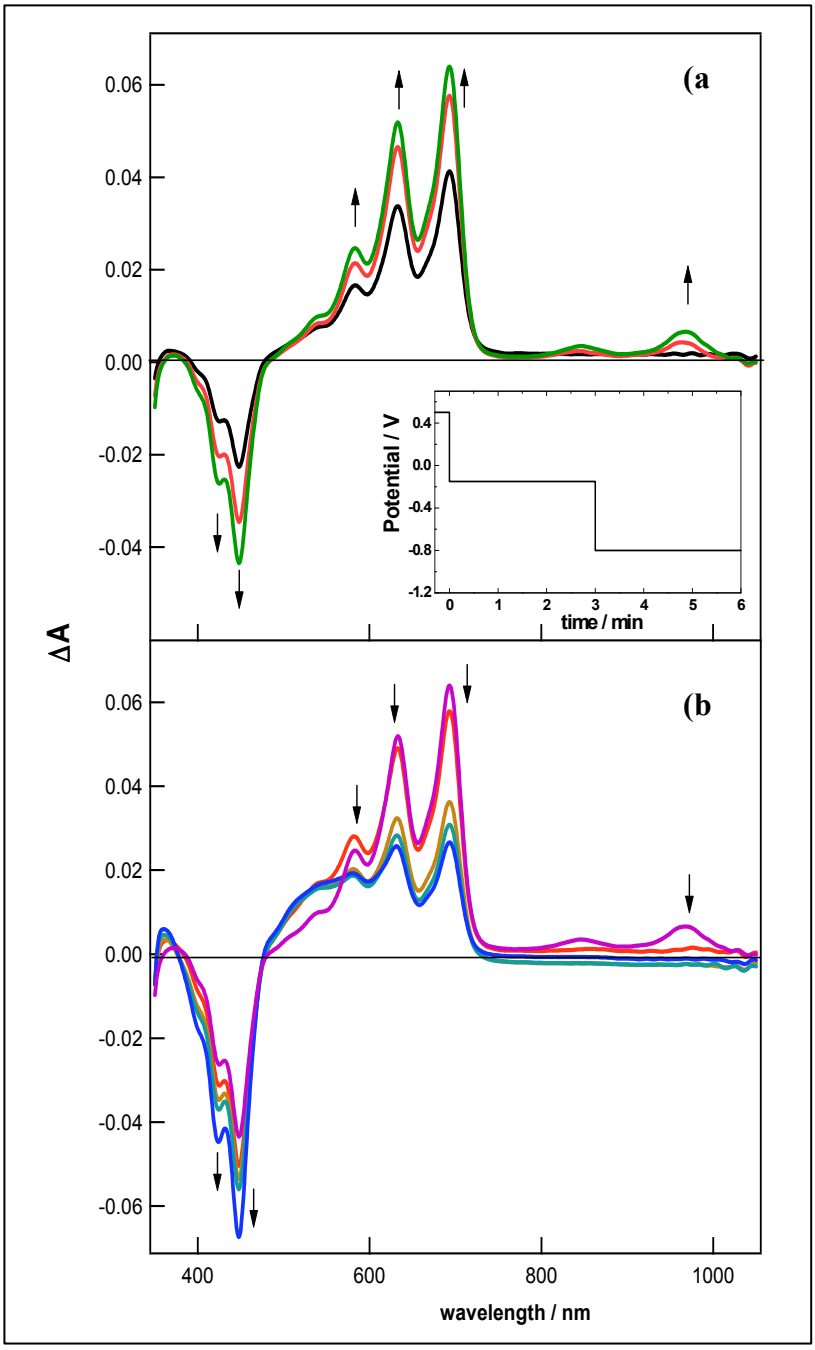


**Figure 5.** Difference absorbance spectra **ΔA** obtained during the electroreduction of Zn-tatpp (60 μM) in MeCN:$H_2O$ 90:10 under two successive potential steps (shown in the inset) from open circuit potential to -0.15 V (a) and from -0.15 V to -0.80 V (b). **ΔA** was obtained by subtracting the spectrum at the initial potential ($E_i$ = 0.50 V) from those obtained at potentials of -0.15 V and -0.80 V respectively. Spectral data were obtained using a transparent ITO film on glass as working electrode.

## Discussion

In complex $\mathbf{1}^{2+}$, the first electroreduced species is radical $\mathbf{1}^{\bullet+}$ which is easily identified by the two long wavelength absorptions at 855 and 960 nm [24]. These bands are clearly discernible in

Fig. 4 as forming (Fig. 4a) and disappearing (Fig. 4b). These peaks are ~1300 $cm^{-1}$ apart in energy and are likely to be the $\nu_{0\text{-}1}$ and $\nu_{0\text{-}0}$ vibronic structure, respectively, of the same electronic transition. Low energy peaks in the electronic spectra are common for aromatic radical anions,[36] which is how we can view the tatpp portion of the complex in $[(bpy)_2Ru(tatpp^{\bullet-})]^{+}$ ($\mathbf{1}^{\bullet+}$). Formation of radical $\mathbf{1}^{\bullet+}$ brings about the bleaching of two Ligand-Centered, LC, absorptions, $LC_1$ at 330 nm and $LC_0$ showing a structured absorption peaking at 450 nm with significant shoulders at 424 nm (Fig. 3 and 4). These absorptions are conveniently interpreted in a localized MO description of the tatpp ligand. $LC_0$ is assigned to a $\pi$-$\pi_0$* transition (tatpp ligand HOMO-LUMO) whereas $LC_1$ is a tatpp HOMO to LUMO+1 transition ($\pi$-$\pi_1$*), as corroborated by the presence of the structured $LC_0$ absorption band in the spectroelectrochemistry of Zn-tatpp adduct (see Figure 5). Importantly, in complex $\mathbf{1}^{2+}$, the tatpp $LC_0$ transition overlaps with a broader Ru(d$\pi$) → ligand ($\pi$*) MLCT transition centered at ca. 450 nm, typical of Ru(II)-phen and bpy type complexes. The net result is an intense band peaking at 450 nm with a molar extinction coefficient of 43,300 $M^{-1}cm^{-1}$.[21]

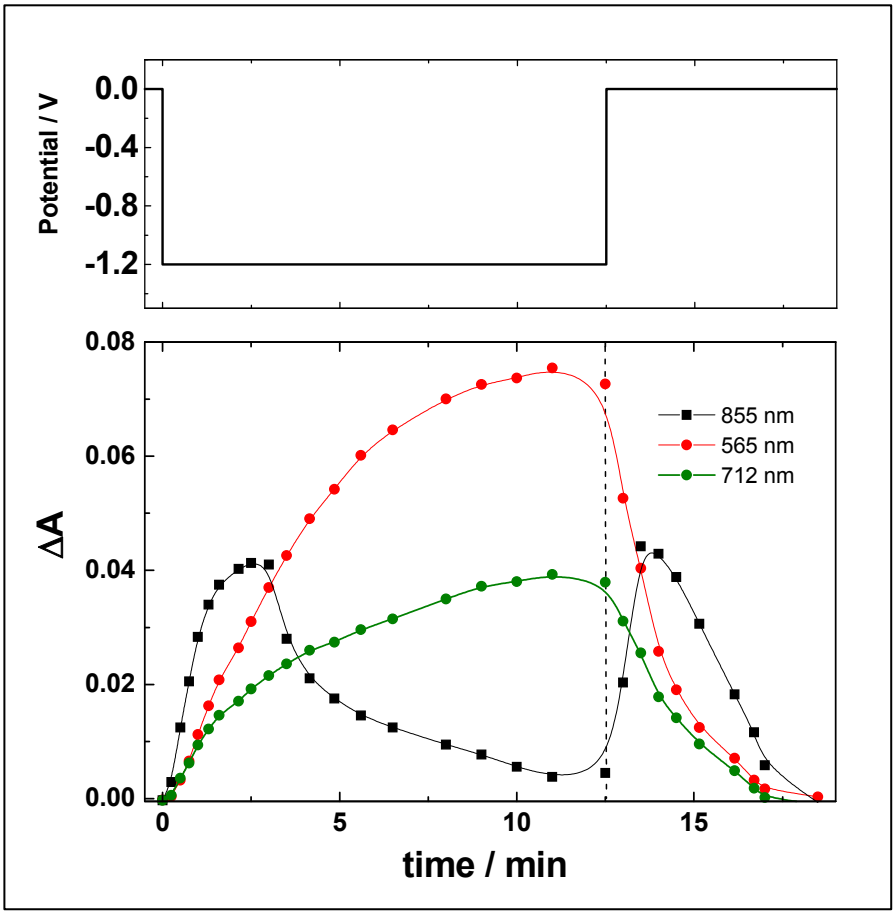


**Figure 6.** **ΔA**-time plots at selected wavelengths (855 nm for $\mathbf{1}^{\bullet+}$, 712 for $H\mathbf{1}^{+}$ and 565 nm for $H_2\mathbf{1}^{2+}$ species respectively) corresponding to the double potential step waveform (0.0 to -1.2 V and back to 0.0 V) shown at the top of the figure. Data were obtained from Figure 4.

The next electroreduction process for radical $\mathbf{1}^{\bullet+}$ is associated with the appearance of a broad band peaking at 565 nm with a shoulder at ca. 710 nm (Figure 4a). This band is made of contributions of doubly reduced, singly-protonated $H_1\mathbf{1}^{+}$ and doubly-protonated $H_2\mathbf{1}^{2+}$species (see Figure 3a). Importantly, the appearance of these absorption bands for singly- and doubly-reduced

species occurs with partial or total disappearance of the tatpp LC transitions (sharp absorptions at 330 nm and 450 nm), because the electroreduction is localized on the tatpp ligand. No bleaching of the characteristic bands of $H_1\mathbf{1}^+$ and $H_2\mathbf{1}^{2+}$ species occurred at constant potentials passing the $C_2$ electroreduction process.

In the Zn-tatpp adduct, minor amounts of radical Zn-(tatpp$^{\bullet-}$) are detected through bands at 855 nm and 960 nm, at potentials encompassing process $C_1$ (Figure 5a). This radical is present in relatively smaller amount than in the electroreduction of complex $\mathbf{1}^{2+}$. In fact, the main electroreduced species upon passing the $C_1$ potential**,** as ascertained by the magnitude of the bands, are those related to doubly-reduced, protonated species, Zn-(Htatpp$^-$) and Zn-($H_2$tatpp). The proton source is the mixed aqueous solvent system. The doubly-reduced species of Zn-tatpp also share spectral similarities with $\mathbf{1}^0$, $H_1\mathbf{1}^+$ and $H_2\mathbf{1}^{2+}$. Protonation of $\mathbf{1}^0$ to give $H\mathbf{1}^+$ and $H_2\mathbf{1}^{2+}$ results in a blue shift of the LC absorption from 692 nm to 565 nm as would be expected from the stabilization of some of the tatpp central nitrogen lone pairs.[37] Upon switching the potential to more negative values so as to emcompass electroreduction process $C_2$, the bands of Zn-(Htatpp$^-$) and Zn-($H_2$tatpp) are seen to bleach (Figure 5b) in contrast with the case of coordinated tatpp as in, e.g. complex $\mathbf{1}^{+2}$.

***Insights in the electroreduction mechanism***

In complex $\mathbf{1}^{2+}$**,** peak $C_1$ is an overall 2 $e^-$/2 $H^+$ process (rxn 1) as $H_2\mathbf{1}^{2+}$ is always the dominant product spectroelectrochemically detected. Reactions 2 through 5 show a number of elementary steps by which reaction 1 can occur. The terms **E** and **C**, given in reactions 2–5, are useful ways of describing a sequential mechanism involving both electrochemical and chemical reactions.[38] Reactions involving ET from the electrode surface are indicated with an **E**, and first-order or pseudo first-order (e.g. protonation) chemical reactions are indicated by a **C**.

$C_1$ overall process: $\mathbf{1}^{2+} + 2e^- + 2H^+ \rightleftarrows H_2\mathbf{1}^{2+}$ (1)

$\mathbf{1}^{2+} + e^- \rightleftarrows \mathbf{1}^{\bullet+}$ **E** (2)

$\mathbf{1}^{\bullet+} + e^- \rightleftarrows \mathbf{1}^0$ **E** (3)

$\mathbf{1}^0 + H^+ \rightleftarrows H\mathbf{1}^+$ **C** (4)

$H\mathbf{1}^+ + H^+ \rightleftarrows H_2\mathbf{1}^{2+}$ **C** (5)

Although process $C_1$ is not resolved into separate peaks; however it encompasses two stepwise one-electron reductions producing first $\mathbf{1}^{\bullet+}$ (rxn 2) and then a mixture of $H\mathbf{1}^+$ and $H_2\mathbf{1}^{2+}$ as detected spectroelectrochemically. The monoreduced $\mathbf{1}^{\bullet+}$ radical is not protonated and its reduction requires first an ET followed by PT as indicated in reactions 3 and 4. $H_2\mathbf{1}^{2+}$ is likely formed predominantly via protonation of $H\mathbf{1}^+$ (rxn 5). As $H_2\mathbf{1}^{2+}$ is the dominant product, this mechanism is largely consistent with an overall $2e^-/2H^+$ process.

At potentials of process $C_2$, a continual build-up of the doubly-reduced product is observed (Figures 4a and 6). However, disappearance of the optical bands for $H\mathbf{1}^+$ and $H_2\mathbf{1}^{2+}$ was clearly seen in potential modulated spectroelectrochemical reported by us elsewhere [24], and supported an overall 2 $e^-$/2 $H^+$ (rxn 6) that brings about the disappearance of doubly-reduced species in the diffusion layer next to the electrode, as follows:

$$H_2\mathbf{1}^{2+} + 2e^- + 2H^+ \rightleftarrows H_4\mathbf{1}^{2+} \quad (6)$$

The product of reaction 6, $H_4\mathbf{1}^{2+}$, would not be expected to show any visible absorption bands due to the complete filling of the LUMO and LUMO+1 molecular orbitals in the protonated forms of the tatpp$^{4-}$ ligand. This was also observed in the related dinuclear complex $H_4\mathbf{2}^{4+}$ which showed a

bleaching of all the visible LC bands.[20] The observation of a continual build-up of $H_2\mathbf{1}^{2+}$ in the spectroelectrochemical experiment (Figures 4 and 6) will afford the formation of $H_4\mathbf{1}^{2+}$, only under the presence of a chemical reaction that rapidly consumes this species and regenerate $H_2\mathbf{1}^{2+}$. This reaction could be a comproportionation reaction of $H_4\mathbf{1}^{2+}$ with $\mathbf{1}^{2+}$ occurring in the bulk of the solution (such as rxn 7).

$$H_4\mathbf{1}^{2+} + \mathbf{1}^{2+} \longrightarrow 2\ H_2\mathbf{1}^{2+} \qquad \textbf{COMP} \qquad (7)$$

The homogeneous electron transfer (rxn 7) between $H_4\mathbf{1}^{2+}$ generated at the interface and bulk $\mathbf{1}^{2+}$ was successfully detected by tracking the fate of electrogenerated $H_2\mathbf{1}^{2+}$ once the potential was interrupted. Figure 7 shows the build-up of $H_2\mathbf{1}^{2+}$ when the potential was disconnected immediately after a linear potential scan from 0.0 V up to -1.2V. Species $H_2\mathbf{1}^{2+}$ was optically tracked at 565 nm during its electrochemical formation (up to -1.2 V, Figure 7a) and after the circuit has been opened (Figure 7b).

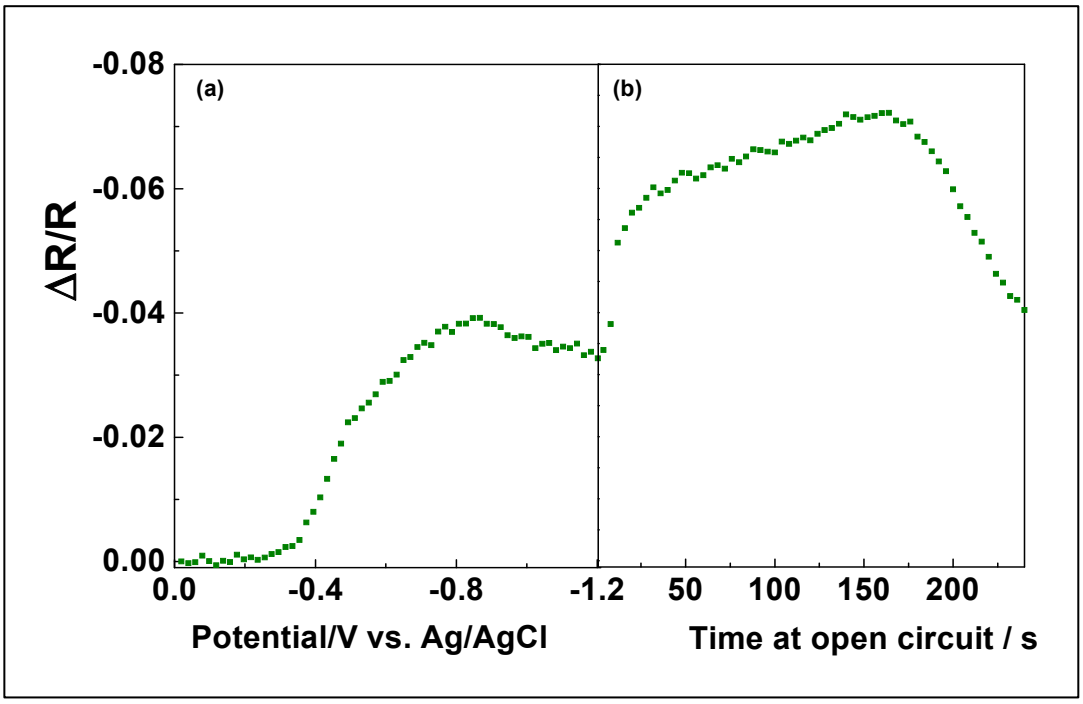


**Figure 7.** Normalized integral reflectance ΔR/R monitoring the generation of $H_2\mathbf{1}^{2+}$ (565 nm) at pH 10.5, during a potential scan from 0.0 V / -1.2 V (encompassing peaks $C_1$ and $C_2$) (frame (a)) and the subsequent evolution of $H_2\mathbf{1}^{2+}$ after the potential had been switched out (frame (b)). Spectra were taken by an OMA system at 4s / 20 mV intervals during the potential scan (5 $mV.s^{-1}$) at open circuit.

Its continuos ***chemical*** formation is observed for ca. 180 s until it diffuses away of the light path. This crucial experiment provides an explanation of the continuous build-up of $H_2\mathbf{1}^{2+}$ species in the spectroelectrochemical data obtained at constant potential passing peak $C_2$ (Figure 4a).

In Zn-tatpp**,** the $C_1$ electroreduction is also associated with a 2-electron process (peak $C_1$ in Fig. 1b) and predominantly forms Zn-($Htatpp^-$) and to a lesser extent, Zn-($H_2$tatpp). The observation

of a small amount of Zn-(tatpp$^{\bullet-}$) during the process suggests its role as an intermediate in the overall process depicted in reactions 8 – 11 (Zn omitted for clarity).

$$\text{tatpp} + e^- \rightleftarrows \text{tatpp}^{\bullet-} \qquad \mathbf{E} \qquad (8)$$

$$\text{tatpp}^{\bullet-} + H^+ \rightleftarrows \text{Htatpp}^{\bullet} \qquad \mathbf{C} \qquad (9)$$

$$2\ \text{Htatpp}^{\bullet} \rightleftarrows \text{tatpp} + \text{H}_2\text{tatpp} \qquad \mathbf{DISP} \qquad (10)$$

$$\text{H}_2\text{tatpp} \rightleftarrows \text{Htatpp}^- + H^+ \qquad \mathbf{C} \qquad (11)$$

The formation Zn-(Htatpp$^{\bullet}$) is preceded by a first electroreduction to Zn-(tatpp$^{\bullet-}$) (detected in minor amounts) which is in equilibrium with Zn-(Htatpp$^{\bullet}$). This latter species is unstable and rapidly disproportionates (rxn 10) to give Zn-(H$_2$tatpp) and Zn-tatpp (Figure 5). Deprotonation of Zn-(H$_2$tatpp) leads to the major product Zn-(Htatpp$^-$).

This behavior contrasts with that of the coordinated tatpp in complex $\mathbf{1}^{2+}$ where the related radical $\mathbf{1}^{\bullet+}$ is seen in relatively much larger amounts, indicating less protonation and therefore, less disproportionation. Thus the $C_1$ process in $\mathbf{1}^{2+}$ is predominantly two sequential one-electron reductions of the complex followed by protonation. In Zn-tatpp the $C_1$ process is also a net two electron process but involves a sequential reduction to a radical anion, protonation, and disproportionation.

At potentials encompassing the $C_2$ process, 2-electron reduction of both $H_2\mathbf{1}^{2+}$ (rxn 6) and Zn-(Htatpp$^-$) (rxn 12) to the quadruply-reduced species is expected to bleach all the visible tatpp-centered optical transitions.

$$\text{Zn-(Htatpp}^-) + 2e^- \rightleftarrows \text{Zn-(Htatpp}^{3-}) \qquad \mathbf{E} \qquad (12)$$

The products of reactions 6 and 12, or some other protonated forms thereof, are not expected to show any visible absorption bands due to the filling of the molecular orbitals, *vide supra*, of the quadruply-reduced tatpp ligand. This was clearly observed for Zn-(Htatpp$^{3-}$) but not with $H_4\mathbf{1}^{4+}$. The reason for this is twofold. In Zn-(Htatpp$^{3-}$), the complex appears to form a film on the ITO electrode surface that restricts its diffusion into the solution. In $H_4\mathbf{1}^{4+}$, the complex is in solution (interface) and diffusion into the bulk leads to comproportionation reaction 7, which was clearly tracked at open-circuit (Figure 7).

## Conclusions

Complex $\mathbf{1}^{2+}$ shows four reversible tatpp-based reductions. The redox processes occur predominantly as two 2 e$^-$/2 H$^+$ processes giving voltammetric peaks $C_1$ and $C_2$ respectively. The $C_1$ voltammetric wave involves the formation of $H\mathbf{1}^+$ and $H_2\mathbf{1}^{2+}$ passing through the intermediate $\mathbf{1}^{\bullet+}$; all the three species are able to be tracked by spectroelectrochemical measurements. The $C_2$ voltammetric wave reflects a double reduction and double protonation leading to the formation of the $H_4\mathbf{1}^{2+}$ product. This species undergoes a rapid comproportionation with $\mathbf{1}^{2+}$ (present in the bulk) leading to its disappearance. Optical measurements performed at open circuit (Figure 7) provided clear evidence of the continual build-up of $H_2\mathbf{1}^{2+}$ through the comproportionation reaction (rxn 7).

The Zn-tatpp adduct undergoes multiple-electron reduction and partial protonation processes involving formation of up to quadruply-reduced species in a rather similar fashion to complex $\mathbf{1}^{2+}$. However, it shows three essential differences with respect to complex $\mathbf{1}^{+2}$:

i) Zn-tatpp species form a film during the electroreduction processes while complex $\mathbf{1}^{2+}$ does not.

ii) Negligible amounts of the first electroreduced species (radical tatpp$^{\bullet-}$) are formed along voltammetric wave $C_1$, while much larger amounts of related radical $\mathbf{1}^{\bullet-}$ were detected during the related electroreduction peak of complex $\mathbf{1}^{2+}$. Both, tatpp$^{\bullet-}$ and $\mathbf{1}^{\bullet-}$ were tracked by the same near-IR

bands, and the lower amounts of Zn-tatpp$^{\bullet-}$ point to the stabilizing effect of the Ru(bpy)$^{2+}$ moiety, probably due to electron donating properties of the two bipyridine ligands.

iii) Facile comproportionation reaction occurring in electroreduction process $C_2$ of complex $\mathbf{1}^{2+}$ contrasting with the absence of this reaction for the Zn-tatpp. Capability of face-to-face encounters is likely responsible for the fast comporportionation reaction while in the second case the capability of the surface-confined species to move for encounter with similar species is inhibited.

Importantly, this paper shows the insights gained by using spectroelectrochemistry in following the electroreduced species of tatpp either as Zn-tatpp adduct or as complex $\mathbf{1}^{2+}$. An understanding of mechanistic details associated with molecular configuration provides a framework by which to describe, and potentially modify, the unusual multi-electron accepting capabilities of the tatpp ligand.

**Acknowledgements.** We thank the National Science Foundation CHE-0518649 (FMM, NRT), the Robert A. Welch Foundation Y-1301(FMM) and BID 1728/OC-RA, PICT #26195/04 (ROL, JMZ) for support of this research.

## References

[1] Armaroli, N.; Balzani, V. *Angew. Chem. Int. Ed.* **2007**, *46*, 52.

[2] Eisenberg, R.; Nocera, D. G. *Inorg. Chem.* **2005**, *44*, 6779.

[3] Alstrum-Acevedo, J. H.; Brennaman, M. K.; Meyer, T. J. *Inorg. Chem.* **2005**, *44*, 6802.

[4] Dempsey, J. L.; Esswein, A. J.; Manke, D. R.; Rosenthal, J.; Soper, J. D.; Nocera, D. G. *Inorg. Chem.* **2005**, *44*, 6879.

[5] Balzani, V.; Ceroni, P.; Maestri, M.; Saudan, C.; Vicinelli, V. *Top. Curr. Chem.* **2003**, *228*, 159.

[6] Sun, L.; Hammarstrom, L.; Akermark, B.; Styring, S. *Chem. Soc. Rev.* **2001**, *30*, 36.

[7] Konduri, R.; Ye, H.; MacDonnell, F. M.; Serroni, S.; Campagna, S.; Rajeshwar, K. *Angew. Chem. Int. Ed.* **2002**, *41*, 3185.

[8] Elvington, M.; Brewer, K. J. *Inorg. Chem.* **2006**, *45*, 5242.

[9] Molnar, S. M.; Nallas, G.; Bridgewater, J. S.; Brewer, K. J. *J. Am. Chem. Soc.* **1994**, *116*, 5206.

[10] Rosenthal, J.; Bachman, J.; Dempsey, J. L.; Esswein, A. J.; Gray, T. G.; Hodgkiss, J. M.; Manke, D. R.; Luckett, T. D.; Pistorio, B. J.; Veige, A. S.; Nocera, D. G. *Coord. Chem. Rev.* **2005**, *249*, 1316.

[11] Heyduk, A. F.; Nocera, D. G. *Science* **2001**, *293*, 1639.

[12] Esswein, A. J.; Veige, A. S.; Nocera, D. G. *J. Am. Chem. Soc.* **2005**, *127*, 16641.

[13] Pfennig, B. W.; Mordas, C. J.; McCloskey, A.; Lockard, J. V.; Salmon, P. M.; Cohen, J. L.; Watson, D. F.; Bocarsly, A. B. *Inorg. Chem.* **2002**, *41*, 4389.

[14] Chang, C. C.; Pfennig, B.; Bocarsly, A. B. *Coord. Chem. Rev.* **2000**, *2008*, 33.

[15] Borgstrom, M.; Shaikh, N.; Johansson, O.; Anderlund, M. F.; Styring, S.; Akermark, B.; Magnuson, A.; L., H. *J. Am. Chem. Soc.* **2005**, *127*, 17504.

[16] Kirmaier, K.; Holten, D. *The Photosynthetic Bacterial Reaction Center - Structure and Dynamics*; Plenum: New York, 1988.

[17] Tommos, C.; Babcock, G. T. *Acc. Chem. Res.* **1998**, *31*, 18.

[18] Huynh, M. H.; Meyer, T. J. *Chem. Rev.* **2007**, *107*, 5004.

[19] Cukier, R. I.; Nocera, D. G. *Ann. Rev. Phys. Chem.* **1998**, *49*, 337.

[20] Konduri, R.; de Tacconi, N. R.; Rajeshwar, K.; MacDonnell, F. M. *J. Am. Chem. Soc.* **2004**, *126*, 11621.

[21] de Tacconi, N. R.; Lezna, R. O.; Konduri, R.; Ongeri, F.; Rajeshwar, K.; MacDonnell, F. M. *Chem. Eur. J.* **2005**, *11*, 4327.

[22] Janaratne, T. K.; Yadav, A.; Ongeri, F.; MacDonnell, F. M. *Inorg. Chem.* **2007**, *46*, 3420.

[23] de Tacconi, N. R.; Chitakunye, R.; Macdonnell, F. M.; Lezna, R. O. *J. Phys. Chem. A* **2008**, *112*, 497.

[24] de Tacconi, N. R.; Lezna, R. O.; Chitakunye, R.; Macdonnell, F. M. *Inorg. Chem* **2008**, *47*, 8847.

[25] Wärnmark, K.; Thomas, J. A.; Heyke, O.; Lehn, J-M. *Chem. Commun.* **1996**, 701.

[26] Bolger, J.; Gourdon, A.; Ishow, E.; Launay, J-P. *Inorg. Chem.* **1996**, *35*, 2937.

[27] Kim, M-J.; Konduri, R.;; Ye, H.; MacDonnell, F.M.; Puntoriero, F.; Serroni, S.; Campagna, S.; Holder, T.; Kinsel, G.; Rajeshwar, K. *Inorg. Chem.* **2002**, *41*, 2471.

[28] Itaya, K.; Uchida, I.; Neff, V. D. *Acc. Chem. Res.* **1986**, *19*, 162.

[29] Kulesza, P. J.; Malik, M. A.; Skorek, J.; Smolinska, A.; Miecznikowski, K.; Zamponi, S.; Berrettoni, M.; Giorgetti, M.; Marassi, R. *J. Electroanal. Chem.* **1999**, *146*, 3757.

[30] de Tacconi, N. R.; Rajeshwar, K.; Lezna, R. O. *Chem. Mater.*, **2003**, *15*, 3046; see also references therein.

[31] Sayyah, S. M.; Abd El-Rehim, S. S.; El-Deeb, M. M. *J. Appl. Polymer Sci.* **2003***, 90,* 1783.

[32] Sadki, S.; Schottland, P.; Brodie, N; Sabouraud, G. *Chem. Soc. Rev.*, **2000**, *29*, 283.

[33] Hong, S. Y.; Jung, Y. M.; Bin Kim, S.; Park, S. M. *J. Phys. Chem. B* **2005**, *109*, 3855.

[34] Gubin, S. P.; Smirnova, S. A.; Denisovich, L. I. *J. Organomet. Chem.* **1971**, *30*, 257.

[35] Koelle, U.; Infelata, P. P.; Grätzel, M. *Inorg. Chem.* **1988**, *27*, 879.

[36] Fox, M. A. *Chem. Rev.* **1978**, *78*, 253.

[37] Turro, N. J. *Modern Molecular Photochemistry*; University Science Books: Sausalito, CA, 1991.

[38] Saveant, J-M. *Elements of Molecular and Biomolecular Electrochemistry - An Electrochemical Approach to Electron transfer Chemistry*; Wiley-Interscience: Hoboken, NJ, 2006.